AIMS Materials Science, 4(1): 1-15.
DOI: 10.3934/matersci.2017.1.1
Received: 30 August 2016
Accepted: 30 November 2016
Published: 13 December 2016

http://www.aimspress.com/journal/Materials

Research article

Precipitation of the metastable phases in a tin microalloyed Al-10at%Ag alloy

Faiza Lourdjane, Mouhyddine Kadi-Hanifi, and Azzeddine Abderrahmane Raho *

Solids solutions laboratory, physics faculty USTHB, BP 32, El-Alia, Algiers, Algeria

* **Correspondence:** Email: raho_azzeddine@yahoo.fr; Tel: +213-21-24-79-50; Fax: +213-21-24-79-04.

Abstract: The formation of the metastable phases in aluminium alloys is closely linked with the excess vacancies. Traces of tin added to an Al-Ag alloy exert an influence on the precipitation kinetics. In the quenched Al-Ag alloys, the precipitation is controlled by the diffusion of solute atoms which require the presence of free vacancies. Due to their high binding energy with vacancies, tin atoms modify the nucleation and growth characteristics of the phases which form during precipitation. Tin atoms retard the precipitation of the Guinier-Preston zones at 90, 125 and 150 °C, suppresses it at 170 and 200 °C and, at all temperatures, stimulate the precipitation of the metastable γ' phase.

Keywords: Al-Ag alloys; Sn addition; metastable phases; precipitation; hardening

1. Introduction

Al-Ag supersaturated solid solution evolves towards the equilibrium state following the sequence [1–4]:

Supersaturated solid solution → Guinier-Preston (GP) zones → metastable γ' phase → equilibrium γ phase

The Guinier-Preston zones (GP), consisting of silver atom clusters, are coherent with the matrix. The metastable γ' (Ag_2Al) phase is semi-coherent with the matrix and the equilibrium γ (Ag_2Al) phase, is incoherent with the matrix. Precipitation starts from the formation of GP zones, which are isomorphous with the matrix and, therefore, have a lower interfacial energy than intermediate or equilibrium precipitate phases which possess a distinct crystal structure. In fact, the GP zones are fully coherent with the matrix and therefore have a very low interfacial energy, whereas the γ' (Ag_2Al) phase is semi-coherent with the matrix which can only form with high-energy semi-incoherent interfaces. Therefore, despite the fact that the driving force for precipitation of GP zones is less than for the metastable γ' (Ag_2Al) phase, the barrier to nucleation is still less, and the zones nucleate most rapidly.

The effect of microalloying elements on the behaviour of age-hardenable alloys, such as, Al-Ag, is an interesting physical problem addressing the mechanisms of transport and aggregation of the solute. Trace elements have been found to exert a disproportionate influence on the structure and properties of Al alloys compared with the amounts added which may be less than 0.1 molar fraction. Most trace element effects arise because they modify the nucleation and the growth characteristics of the phases which form during precipitation such the GP zones and the metastable γ' phase in the case of Al-Ag alloys [5–9]. It is well known that the formation of the GP zones in aluminium alloys is closely linked with the excess vacancies. A number of model of GP zones precipitation assisted by vacancies has been developed by several authors [10,11,12]. GP zones formation is governed by a transport mechanism of solute atoms by solute atom-vacancy complexes. The high binding energy between tin atoms and vacancies leads to the formation of vacancy-tin atom pairs and silver atom-vacancy-tin atom complexes.

In a supersaturated Al-Ag alloy, the precipitation of the GP zones and the metastable γ' phase is responsible of a variation of the physical properties of the alloy and particularly, the mechanical properties. The evolution of all these properties is linked with the nature of the precipitate particles and their precipitation kinetics. Our purpose is to study the effect of the addition of traces of tin on the precipitation of the GP zones and the metastable γ**'** phase in Al-10at%Ag alloy using a method based on hardness measurements and differential scanning calorimetry.

2. Materials and Method

Al-10at%Ag (31wt%) and Al-10at%Ag-0.05at%Sn (2wt%) alloys were prepared by melting 99.99%, 99.99% and 99.99% pure aluminum, silver and tin, respectively, under argon protection. After homogenization 15 days at 540 °C and ice water quenching, the alloys are cut into platelet specimens which are mechanically polished, homogenized 6 hours at 540 °C and quenched into ice water. A P1710 Phillips X-ray ray powder diffractometer, utilizing the monochromatic CuKα1 radiation, is used for the characterization of our alloys. The Vickers microhardness measurements were carried out under a load of 100 g on specimen treated during different times at different aged temperatures (90, 125, 150, 170, and 200 °C) and quenched into ice water. The Vickers hardness measurements were made using a microhardness tester type SHIMADZU provided with a square pyramidal penetrator. The differential scanning calorimetry analysis, using a NETZSCH 200 PC

DSC microcalorimeter, were performed on disk shape of 4 mm diameter and 3 mm thickness. The thermal cycle applied consists of a heating with a rate of 5 °C·min^{-1}.

3. Results and Discussion

3.1. Characterization of the Solid Solutions

The as quenched solids solutions, Al-Ag and Al-Ag-Sn, are characterized by X-ray diffraction on powder specimen. It is well known that an as quenched substitutional solid solution is in a disordered state. In the case of aluminium based solids solutions, the X-ray ray powder diffraction spectra give peaks diffraction at the analogous positions of those given by the aluminium. The Al, Al-Ag and Al-Ag-Sn powder diffraction spectra show that the successive peaks are at analogous positions (Figure 1) and their integrated intensities vary in the same ratio (Table 1). The lattice parameters of Al, Al-Ag and Al-Ag-Sn, determined using the Nelson-Riley [13] extrapolation function, are 4.0462 Å, 4.0478 Å and 4.0467 Å with an error estimated at 0.05% respectively. In such a case, there is practically no difference between these lattice parameters. This is due to the fact that there is a little difference between the Al and the Ag atomic radius and the Sn, which have a larger atomic radius, is added in traces proportion.

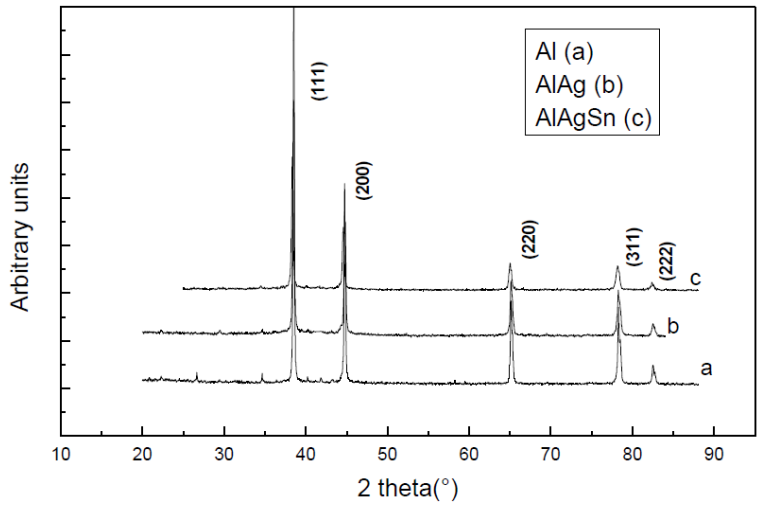

Figure 1. X-ray diffractograms of Al, Al-Ag and Al-Ag-Sn as quenched solid solutions.

Table 1. Integrated intensities ratios.

hkl	Al (I_{hkl}/I_{111})	Al-Ag (I_{hkl}/I_{111})	Al-Ag-Sn (I_{hkl}/I_{111})
111	100	100	100
200	50	51	53
220	21	30	29
311	20	21	21
222	6	6	6

3.2. Hardening Evolution at 90, 125 and 150 °C

The isotherm curves of hardness, established at 90, 125 and 150 °C show a first step of hardening due to the GP zones precipitation and a second step due to the precipitation of the metastable γ' phase (Figures 2, 3 and 4). The obtained degree of hardening depends on the volume fraction, the structure of the precipitates and the nature of the interface between the metastable phases and the aluminum matrix [10,14–19].

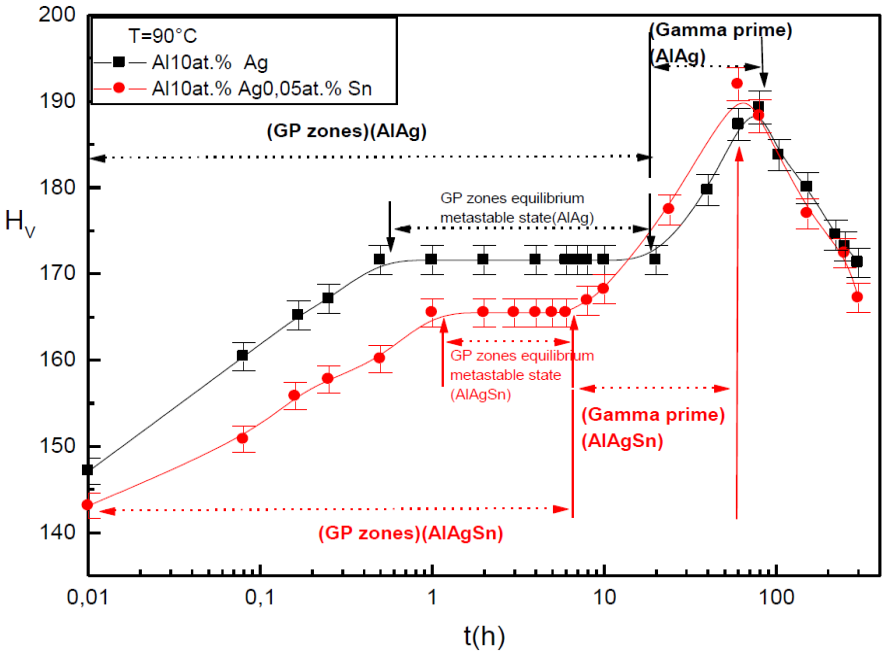

Figure 2. Isotherm hardness curves at 90 °C.

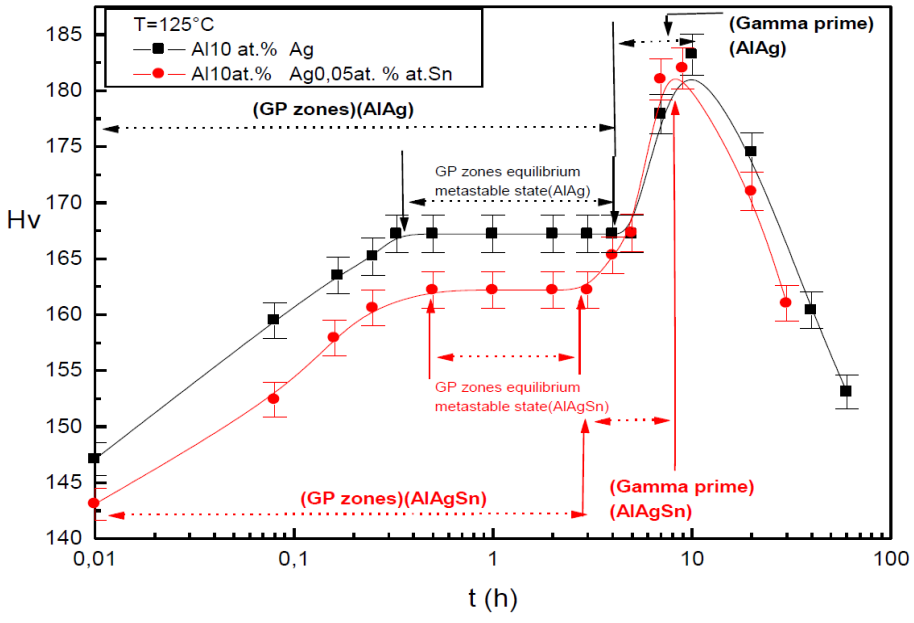

Figure 3. Isotherm hardness curves at 125 °C.

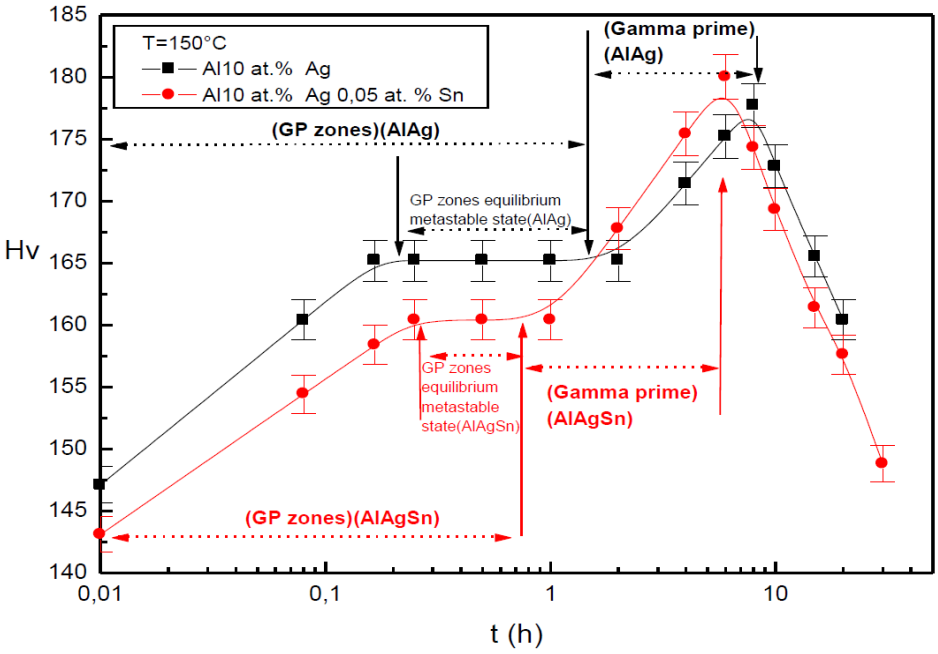

Figure 4. Isotherm hardness curves at 150 °C.

The intermediate bearing corresponds to the metastable equilibrium state of the precipitation of the GP zones during which their volume fraction is maximum. The softening is due to the coarsening of the particles of the γ' phase and to the precipitation of the equilibrium γ phase. These isotherm curves of hardness show that tin atoms retard the establishment of the metastable equilibrium state of the GP zones precipitation by trapping some of quenched in vacancies. Due to the high binding energy between tin atoms and vacancies, tin atom-vacancy pairs and silver atom-vacancy-tin atom complexes are formed, thus reducing the number of free vacancies available to promote the diffusion of Ag atoms for the formation of the GP zones.

Due to the relatively high binding energy between tin atoms and vacancies, estimated to be about 0.43 eV [20,21] , compared with that of the silver atoms-vacancy binding energy , estimated to be about 0.25 eV [22], tin atom-vacancy pairs [23,24] are formed and, due to the strong interaction between the tin atoms and the vacancies and the interaction between the silver atoms and the vacancies, silver atom-vacancy-tin atom complexes are formed, thus reducing the number of free vacancies available to promote the diffusion of Ag atoms for the formation of the GP zones.

These curves also show that tin addition stimulates the precipitation of the metastable γ' phase. This is due to the fact that tin atoms are absorbed at the interface γ'-matrix and reduce the interfacial energy required for precipitate nucleation [25,26]. An alternative explanation is that the clustering of tin elements, which have a larger atomic volume than matrix aluminium, would create a compressive volume strain in the matrix, thus attracting a high concentration of vacancies and silver atoms to the interfacial region, providing an excellent condition for the nucleation of the metastable γ' phase [27].

3.3. Precipitation Kinetics of the GP Zones

During the precipitation of the GP zones, the transformed fraction, F, which represents the ratio

between the volume occupied by the GP zones at a time t and their volume at the metastable equilibrium state, is given by the Merle relatio [28]:

$$H_v(t) = F \cdot H_{v(\text{metastable equilibrium})} + (1 - F) \cdot H_v(0)$$

where $H_v(0)$ is the as quenched hardness, $H_v(t)$ is the hardness of the alloy at the time t during the precipitation of the GP zones, and $H_{v(\text{metastable equilibrium})}$, the hardness of the alloy at the metastable equilibrium state of the GP zones precipitation. The incubation times, which the determined values by extrapolation varies between 0.01 and 0.02 hours, compared with the necessary times to reach the metastable equilibrium state, are very short and are characteristics of a rapid nucleation in the two both alloys, Al-Ag and Al-Ag-Sn, because of the high supersaturation of the quenched in vacancies (Figures 5, 6 and 7).

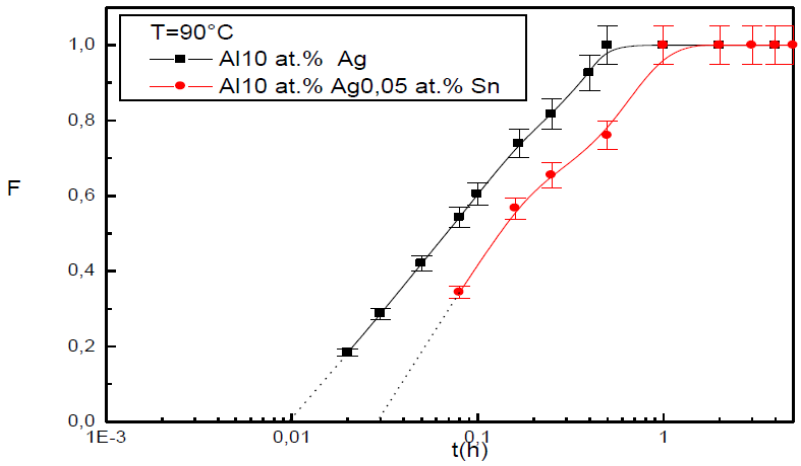

Figure 5. Transformed fraction during GP zones precipitation in Al-Ag and Al-Ag-Sn alloys at 90 °C.

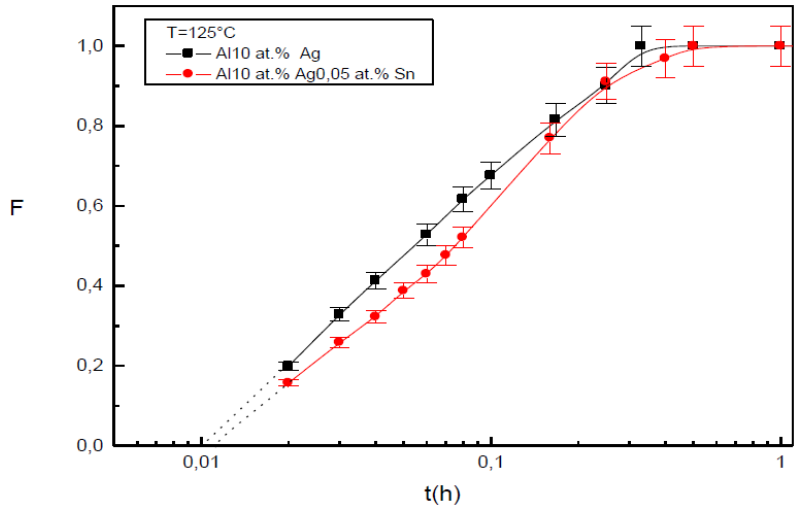

Figure 6. Transformed fraction during GP zones precipitation in Al-Ag and Al-Ag-Sn alloy at 125 °C.

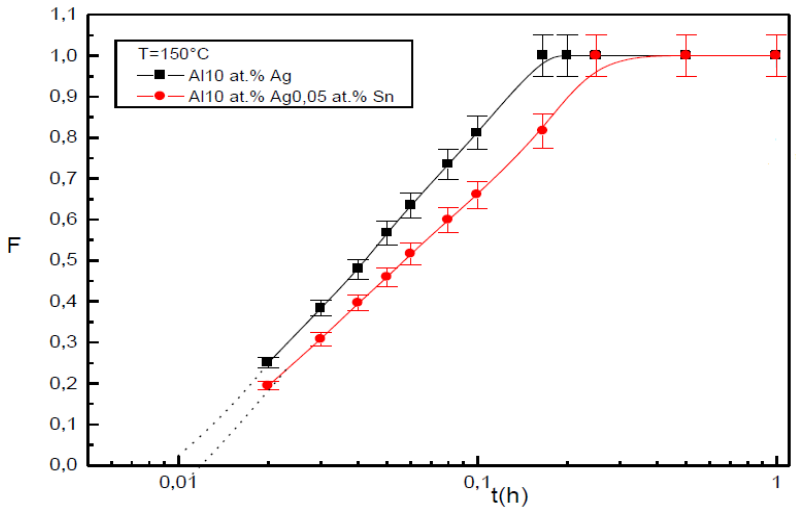

Figure 7. Transformed fraction during GP zones precipitation in Al-Ag and Al-Ag-Sn alloy at 150 °C.

The curves of the variations of ln(ln(1/1 − F)) versus ln(t), show that the growth stage obeys to the JMAK (Johnson-Mehl-Avrami-Kolmogorov) [29,30,31] law, $F = 1 - exp[(-kt)^n]$, of the growth controlled by solute atom diffusion, where n and k are the growth parameters (Figures 8, 9 and 10).

The values of n are characteristics of a heterogeneous precipitation in the two alloys while the values of k, which characterizes the transformation kinetic, show a delay of the precipitation of the GP zones in Al-Ag-Sn alloy (Table 2).

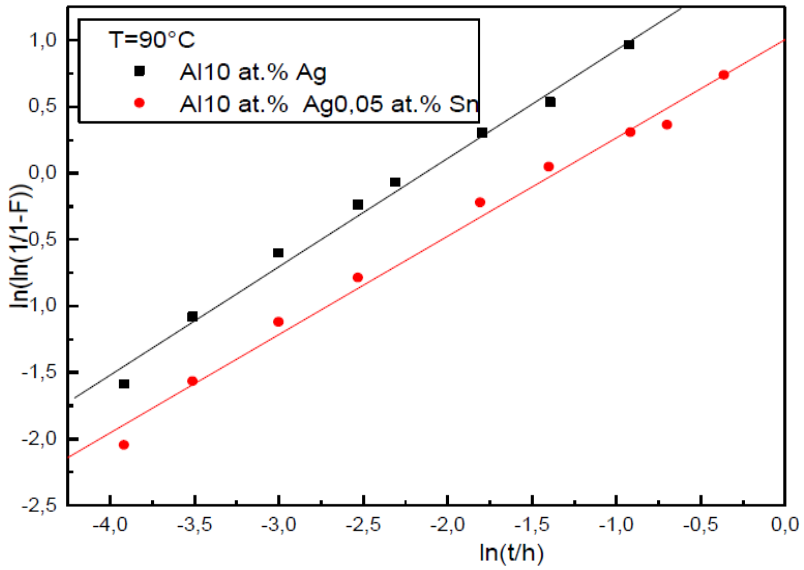

Figure 8. Determination of the growth parameters for Al-Ag and Al-Ag-Sn alloys at 90 °C.

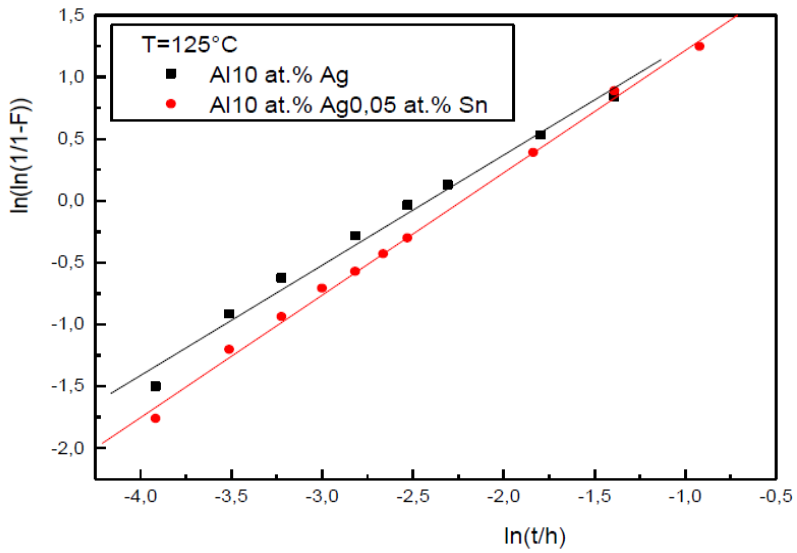

Figure 9. Determination of the growth parameters for Al-Ag and Al-Ag-Sn alloys at 125 °C.

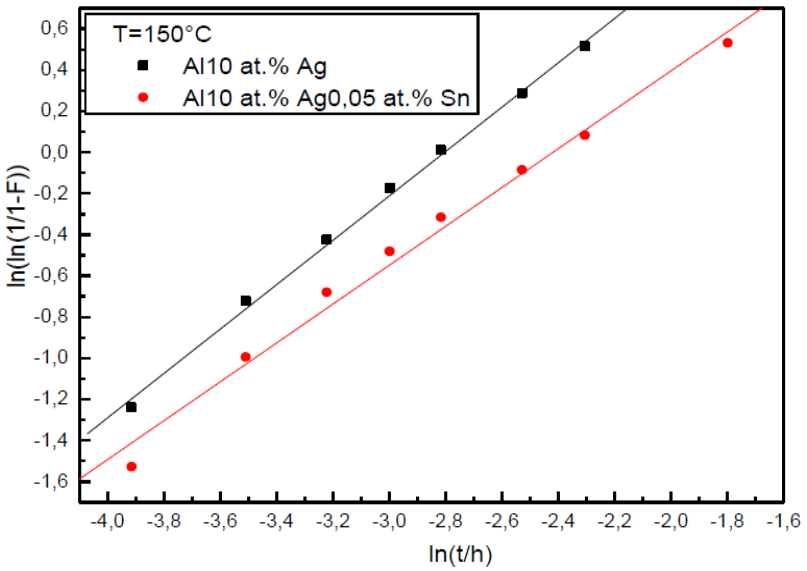

Figure 10. Determination of the growth parameters for Al-Ag and Al-Ag-Sn alloys at 150 °C.

Table 2. Values of the growth parameters.

T (°C)	Al-Ag		Al-Ag-Sn	
	n	k (s^{-1})	n	k (s^{-1})
90	0.80	22×10^{-4}	0.84	10×10^{-4}
125	0.82	31×10^{-4}	1.0	24×10^{-4}
150	1.08	44×10^{-4}	0.94	30×10^{-4}

3.3.1. Activation Energy

The apparent activation energy, Q, is determined using the Arrhenius law $k = A \cdot exp(-Q/RT)$ [32] where A is a constant, T is the temperature and R is the gas constant. The slopes of the variation curves ln(k) = f(1/T) (Figure 11) gives an apparent activation energy in the order of 14 ± 1.4 kJ/mol and 24 ± 2.4 kJ/mol in the Al-Ag and the Al-Ag-Sn alloys respectively corresponding to a difference of 10 kJ/mol (0.1 eV) which confirms that the reaction of GP zones precipitation is slowest in the microalloyed alloy.

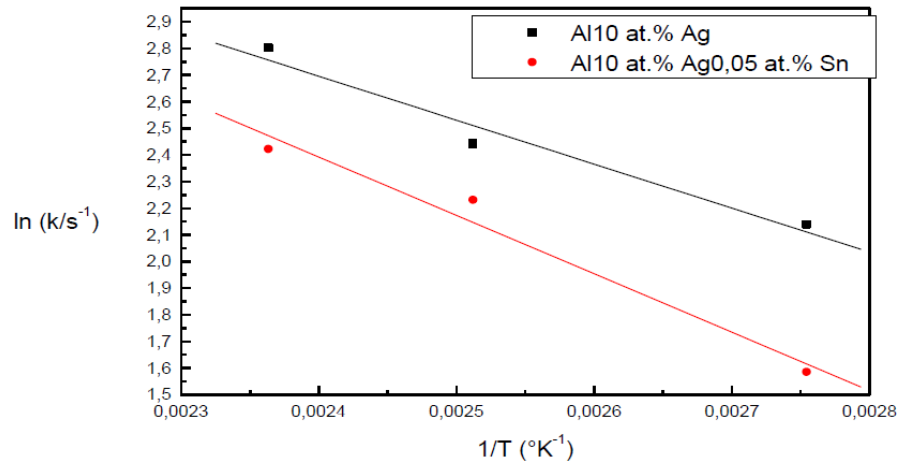

Figure 11. Determination of the difference between activation energy in Al-Ag and Al-Ag-Sn alloys.

3.4. Precipitation of the Metastable γ' Phase

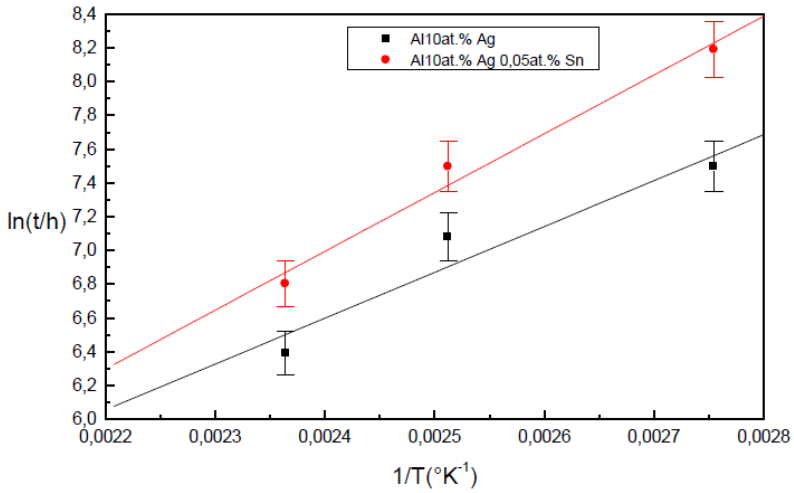

Figure 12. Variation of the duration of the GP zones equilibrium metastable state, Δt.

At 90, 125 and 150 °C, the isotherm curves of hardness show that tin addition stimulates the precipitation of the metastable γ' phase. The variations of the duration of the GP zones equilibrium metastable state, Δt, and the beginning time of the second step hardening which corresponds to the γ' particles precipitation, $t_{\gamma'}$, against 1/T obey to an Arrhenius type law $A \cdot exp(-Q/RT)$, where A is a constant, T is the temperature and R is the gas constant (Figures 12 and 13).

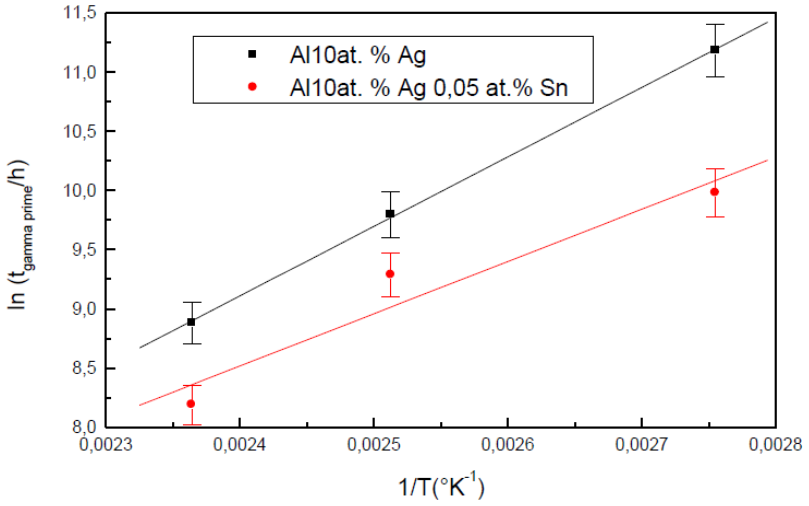

Figure 13. Variation of the beginning time of the second step hardening, $t_{\gamma'}$.

The apparent activation energies of the solute atom diffusion, determined from the slopes of these variations curves, show that the precipitation of the γ' phase occurs earlier in the Al-Ag-Sn alloy (Table 3).

Table 3. Apparent activation energies determined from the duration of the GP zones equilibrium metastable state, Δt variation and from the beginning time of the second step hardening $t_{\gamma'}$ variation .

Alloy	Al-Ag	Al-Ag-Sn
Q (kJ/mol) (Δt)	50.1 ± 5.0	38.7 ± 3.9
Q (kJ/mol) ($t_{\gamma'}$)	48.8 ± 4.9	36.7 ± 3.7

The difference between these apparent activation energies, $\Delta Q = Q_{Al\text{-}Ag} - Q_{Al\text{-}Ag\text{-}Sn}$, of the solute atom diffusion in Al-Ag and in Al-Ag-Sn alloys, determined from the Δt variation (Figure 12) and from the $t_{\gamma'}$ variation (Figure 13) are in the order of 11.4 ± 1.1 kJ/mol (0.11 ± 0.01 eV) and 12.1 ± 1.2 kJ/mol (0.12 ± 0.01 eV) respectively.

It is explained by the fact that tin atoms are absorbed at the interface γ'-matrix and reduce the interfacial energy required for precipitate nucleation [25,26]. An alternative explanation is that the clustering of tin elements, which have a larger atomic volume than the aluminium matrix, would create a compressive volume strain in the matrix, thus attracting a high concentration of vacancies

and silver atoms to the interfacial region, providing an excellent condition for the nucleation of the metastable γ' phase [27].

3.4.1. Precipitation at 170 °C and 200 °C

In the added alloy, the isotherm curves of hardness established at 170 °C and 200 °C (Figures 14 and 15) show, in a first stage, a light softening due, probably, to the coarsening and the dissolution of the GP zones as soon as the nuclei of the γ'phase, more thermodynamically stable, appear as observed on the DSC curves (Figure 16). At this stage, the particle size of the γ' phase produces an insufficient hardening [10,14–19]. In the second stage, the hardening is due to the growth of the particles of the γ' phase.

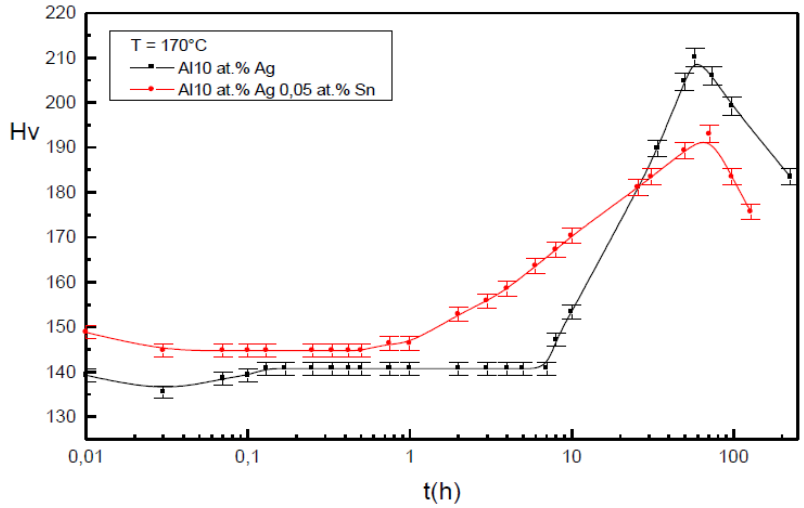

Figure 14. Isotherm curves of hardness at 170 °C.

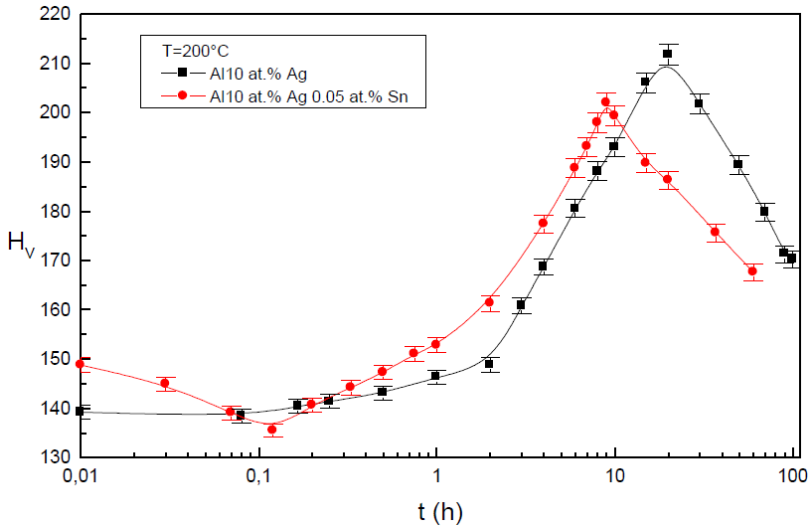

Figure 15. Isotherm curves of hardness at 200 °C.

In the non added alloy, as well as 170 °C and 200 °C, due to the thermal activation, it the GP zones are rapidly formed and their equilibrium metastable state, which is reached rapidly, is followed by their dissolution and the formation of the γ' phase which hardens the alloy as shown in the DSC curves (Figure 16) [10,14–19]. The differential scanning calorimetry (DSC) curves where we observe two peaks (Figure 16). The first one, endothermic, between 150 °C and 200 °C for Al-Ag alloy and between 150 °C and 180 °C for Al-Ag-Sn alloy, corresponds to the dissolution of the GP zones. The second one, exothermic, between 240 °C and 325 °C for Al-Ag alloy and between 225 °C and 310 °C for Al-Ag-Sn, corresponds to the precipitation of the metastable γ' phase. The energy associated with the dissolution of the GP zones and that associated with the precipitation of the γ' metastable phase are given by the peak area in the Table 4. The peaks temperature and the peak area are given in the Table 4.

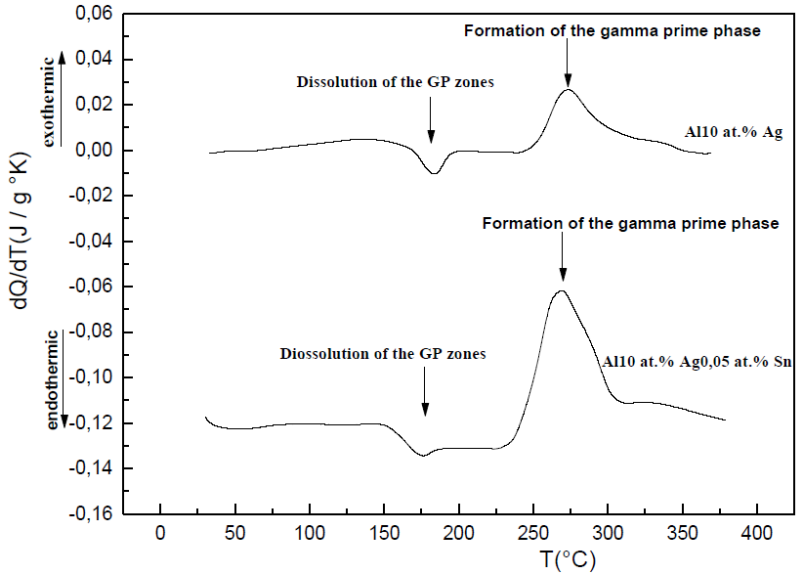

Figure 16. DSC thermograms of Al-Ag and Al-Ag-Sn alloys at the heating rate of 5 °C/mm.

Table 4. DSC results.

Alloy	GP zones dissolution		γ' phase precipitation	
	Peak (°C)	Peak area (J/g)	Peak (°C)	Peak area (J/g)
Al-Ag	183	0.28	273	1.04
Al-Ag-Sn	176	0.35	269	2.69

In results, the presence of tin atoms in the alloy prevents the formation of the GP zones and promotes the precipitation of the γ' phase by trapping vacancies. In fact, at an early stage of aging treatment, due to the high binding energies between the tin atoms and vacancies, tin atom-vacancy and tin atom-vacancy-silver atom clusters are formed [20–24], thus effectively reducing the number of free vacancies available to promote the diffusion of Ag atoms for the formation of the GP zones,

and consequently, suppressing the formation of the GP zone and promoting the precipitation of the γ' metastable phase [29,33] .

4. Conclusion

In the Al-10at%Ag-0.05at%Sn alloy, tin atoms form tin atom-vacancy pairs and tin atom-vacancy-silver atom complexes which retards the precipitation of the GP zones at low temperatures (90, 125, 150 °C) and suppress their precipitation at higher temperatures (170, 200 °C). At all temperatures, the presence of tin atoms stimulates the precipitation of the metastable γ' phase.

Conflict of Interest

The authors declare that there is no conflict of interest regarding the publication of this manuscript.

References

1. Inoke K, Kaneko K (2006) Severe local strain and the plastic deformation of Guinier Preston zones in the Al-Ag system revealed by three-dimensional electron tomography. *Acta Mater* 54: 2957–2963.
2. El-Khalek AMA (2008) Transformation characteristics of Al-Ag and Al-Ag-Ti alloys. *J Alloy Compd* 459: 281–285.
3. Dubey PA (1991) Shape and internal structure of Guinier-Preston zones in Al-Ag. *Acta Metall Mater* 39: 1161–1170.
4. Schönfeld B, et al. (1997) Guinier-Preston zones in Al-rich Al-Cu and Al-Ag single crystals. *Physica B 234:* 983–985.
5. Kimura H, Hasiguti RK (1961) Interaction of vacancies with Sn atoms and the rate of GP zone formation in an Al-Cu-Sn alloy. *Acta Metall* 9: 1076–1078.
6. Nuyten JBM (1967) Quenched structures and precipitation in Al-Cu alloys with and without trace additions of Cd. *Acta Metall* 15: 1765–1770.
7. Noble B (1968) Theta-prime precipitation in aluminium-copper-cadmium alloys. *Acta Metall* 16: 393–401.
8. Ozbilen O, Flower HM (1989) Zirconium-vacancy binding and its influence on S' precipitation in an Al-Cu-Mg alloy. *Acta Metall* 37: 2993–3000.
9. Mukhopadhyay AK, et al. (1990) Role of vacancies on the precipitation processes in Zr modified aluminium based alloys. *Scripta Metall Mater* 24: 307–312.
10. Federighi T (1958) Quenched-in vacancies and rate of formation of zones in aluminum alloys. *Acta Metall* 6: 379–381.
11. Federighi T, Thomas G (1962) The interaction between vacancies and zones and the kinetics of pre-precipitation in Al-rich alloys. *Phil Mag* 7: 127–131.
12. Girifalco LA, Herman H (1965) A model for the growth of Guinier-Preston zones-the vacancy pump. *Acta Metall* 13: 583–590.

13. Nelson JB, Riley DB (1945) An experimental investigation of extrapolation methods in the derivation of accurate unit-cell dimensions of crystals. Proceedings of the Physical Society 57: 160–177.
14. Guo Z, Sha W (2005) Quantification of precipitate fraction in Al-Si-Cu alloys. *Mater Sci Eng A* 392: 449–452.
15. Waterloo G, Hansen V, Gjonnes J, et al. (2001) Effect of predeformation and preaging at room temperaure in Al-Zn-Mg-(Cu, Zr) alloys. *Mater Sci Eng A* 303: 226–233.
16. Wang G (2007) Influence of Cu content on ageing behavior of AlSiMgCu cast alloys. *Mater Design* 28: 1001–1005.
17. Novelo-Peralta O (2007) Characterization of precipitation in Al-Mg-Cu alloys by X-ray diffraction peak broadening analysis. *Mater Charact* 59: 773–780.
18. Shokuhfar A (2009) Mechanisms of precipitates formation in an Al-Cu-Li-Zr alloy using DSC technique and electrical resistance measurements. *Iran J Mater Sci Eng* 6: 15–20.
19. Anjabin N, Taheri AK (2010) The effect of aging treatment on mechanical properties of AA6082 alloy: modelling experiment. *Iran J Mater Sci Eng* 7: 14–21.
20. Hashimoto F, Ohta M (1964) Interaction between a Vacancy and an Si, Ge or Sn Atom in Al-10wt%Zn Alloys. *J Phys Soc Jpn* 19: 1331–1336.
21. Ohta M, Hashimoto F (1964) Interaction between a Vacancy and a Cd or In Atom in Al-10wt%Zn Alloys. *J Phys Soc Jpn* 19: 1987–1987.
22. Hashimoto F (1965) Interaction between a Vacancy and an Ag Atom in Aluminium. *J Phys Soc Jpn* 20: 336–346.
23. Fiorito G, Ceresara S, Federighi T (1966) Interaction between vacancies and Sn atoms in cold-worked Al-Sn alloys. *Acta Metall* 14: 452–454
24. Kimura H, Hasiguti RR (1963) Proc. Int. Conf. Cryst. Latt. Def. (1962). *J Phys Soc Jpn* 18: 73.
25. Silcock JM (1955) The structural ageing characteristics of ternary aluminium-copper alloys with cadmium, indium or tin. *J I Met* 84: 23–31.
26. Sankaran R, Laird C (1974) Effect of trace additions Cd, In and Sn on the interfacial structure and kinetics of growth of θ' plates in Al-Cu alloy. *Mater Sci Eng* 14: 271–279.
27. Schueller RD, Wawner FE (1994) Nucleation mechanism of the cubic σ-phase in squeeze-cast aluminium matrix composites. *J Mater Sci* 29: 424–435.
28. Merlin J, Merle P (1978) Anelastic phenomena and structural state in aluminium silver alloys. *Scripta Metal* 12: 227–232.
29. Johnson WA, Mehl RF (1939) Reaction kinetics in processes of nucleation and growth. *Trans Amer Inst Mining (Metal) Engrs* 135: 416–458
30. Avrami M (1941) Kinetics of phase change. III: Granulation, Phase Change and Microstructure. *J Chem Phys* 9: 177–184.
31. Kolmogorov AN (1937) On the statistical theory of the crystallization of metals. *Bull Acad Sci USSR, Math Ser* 1: 355–359.
32. Esmaeili S, Lloyd DJ, Poole WJ (2003) A yield strength model for the Al-Mg-Si-Cu alloy AA6111. *Acta Mater* 51: 2243–2257.

33. Sofyan BT (2001) Effects of microalloying with Cd and Ag on the precipitation process of Al-4Cu-0.3Mg(wt%) alloy at 200 °C. *Micron* 32: 851–856.